Quantifying effects of long-range transport of NO₂ over Delhi using back-trajectories and satellite data

Ailish M. Graham[1,2], Richard J. Pope[1,2], Martyn P. Chipperfield[1,2], Sandip S. Dhomse[1,2], Matilda
Pimlott[1], Wuhu Feng[1,3], Vikas Singh[4], Ying Chen[5,6], Oliver Wild[7], Ranjeet Sokhi[8], Gufran Beig[9]

[1]School of Earth and Environment, University of Leeds, Leeds, LS2 9JT, UK
[2]National Centre for Earth Observation, University of Leeds, Leeds, LS2 9JT, UK
[3]National Centre for Atmospheric Science, University of Leeds, Leeds, LS2 9PH, UK
[4]National Atmospheric Research Laboratory, Gadanki, India
[5]Laboratory of Atmospheric Chemistry, Paul Scherrer Institute, 5232 Villigen PSI, Switzerland
[6]School of Geography, Earth and Environmental Sciences, University of Birmingham, Birmingham,
B15 2TT, UK
[7]Lancaster Environment Centre, Lancaster University, Lancaster, LA1 4QY, UK
[8]Centre for Climate Change Research (C3R), School of Physics, Engineering and Computer Science,
University of Hertfordshire, Hatfield, AL10 9AB, UK
[9]National Institute of Advanced Studies, Indian Institute of Science Campus, Bangalore-560012, India

Correspondence to: Ailish M. Graham (A.M.Graham@leeds.ac.uk)

Abstract.

Exposure to air pollution is a leading public health risk factor in India, especially over densely populated Delhi and the surrounding Indo-Gangetic Plain. During the post-monsoon months, the prevailing north-westerly winds are known to influence aerosol pollution events in Delhi, by advecting pollutants from agricultural fires as well as from local sources. Here we investigate the year-round impact of meteorology on gaseous nitrogen oxides ($NO_x = NO + NO_2$), a hazardous primary air pollutant for health, which can lead to the formation of secondary aerosols and ozone. We use bottom-up NO_x emission inventories (anthropogenic and fire) and high-resolution satellite measurement based tropospheric column NO_2 ($TCNO_2$) data, from S5P on-board TROPOMI, alongside a back-trajectory model (ROTRAJ) to investigate the balance of local and external sources influencing air pollution changes in Delhi, with a focus on different emission sectors. Our analysis shows that accumulated emissions (i.e. integrated along the trajectory path, allowing for chemical loss) are highest under westerly, north-westerly and northerly flow during pre- (February - March) and post- (October - January) monsoon periods. During the pre-monsoon period, the residential and transport sectors together account for more than 50% of the total accumulated emissions, which are dominated by local sources (90%) under easterly winds and by non-local sources (>70%) under north-westerly winds. The high accumulated emissions estimated during the pre-monsoon season under north-westerly wind directions are likely to be driven by high NO_x emissions locally and in nearby regions (since NO_x lifetime is reduced and the boundary layer is relatively deeper in this period). During the post-monsoon period non-local (60%) transport emissions are the largest contributor to the total accumulated emissions as high emissions, coupled with a relatively long NO_x atmospheric lifetime and shallow boundary-layer aid the build-up of emissions along the trajectory path. Analysis of surface daily NO_2 observations indicates that high pollution episodes (> 90th percentile) occur predominantly in the post-monsoon and more than 75% of high pollution events are primarily caused by non-local sources. Overall, we find that in the post-monsoon period, there is a substantial import of NO_x pollution into Delhi with a large contribution from the transport sector. This work indicates that the advection of highly polluted air originating from outside Delhi is of concern for the population and air quality mitigation strategies need to be adopted not only in Delhi but in the surrounding regions to successfully control this issue. In addition, our analysis suggests that the largest benefits to Delhi NO_x air

quality would be seen with targeted reductions in emissions from the transport sector, particularly during post-monsoon months.

50 **1 Introduction**

The Indo-Gangetic Plain (IGP) covers ~20% of the Indian subcontinent geographical area and houses almost 40% of the population, producing >40% of the total food grain (Badarinath et al., 2009). Within the region, much of the agricultural land is used for rice and wheat production, with ~12 million ha in a wheat-rice crop pattern (Badarinath et al., 2009). Each year there are two major growing seasons; rice is
55 grown from May-September, with harvesting in October-November, and wheat is grown from November-April, with harvesting in April-May. Since the 1980s there has been a shift towards machine harvesting of crops (Badarinath et al., 2009; Jethva et al., 2019). However, this method leaves a large portion of the crop stem root-bound and difficult to remove quickly before sowing the next crop. Wheat stubble is valued for animal feed and a considerable fraction is removed for this purpose before burning. However, rice
60 stubble is generally burned to clear the land quickly as burning is more economically viable than manual removal (Ahmed et al., 2015). Recently Kumar *et al.* (2021) estimated that a total of ~17,000 Tg of rice stubble is burnt each year in India. As a result, burning of rice stubble in the north-west IGP alone accounts for almost 85% of biomass burning in India seasonally and almost 20% annually (Jethva et al., 2019).

65 The timing of agricultural waste burning has shifted over the past decade due to the introduction of the Subsoil Water Act (SSWA). The SSWA was passed by the government of Punjab in 2009 and requires farmers to delay sowing and transplantation of rice until mid-May and mid-June, respectively (Singh, 2009). The law was introduced to reduce ground water demand by bringing the rice-growing season into line with the arrival of the summer monsoon rainfall (Singh, 2009). However, the SSWA shortened the
70 time period between rice harvest and wheat sowing, resulting in an increased reliance on rice stubble burning to clear land more quickly (Jethva et al., 2019). This has been observed through shifts in the timing of burning from early to late October and an increase in the prevalence of fires (Sembhi et al., 2020; Kant et al., 2022; Liu et al. (2021)).

75 During the post-monsoon months of October and November synoptic meteorology is favourable for the advection of air pollution from agricultural burning towards Delhi and surrounding areas (e.g. Mor et al., 2022; Jethva et al., 2018). Bikkina *et al.* (2019) performed cluster analysis of back-trajectories released from Delhi and found that north-west IGP emissions have a large (80-100%) influence on air quality in Delhi during autumn (October–November) and winter months (January–February). Additionally, a
80 shallow boundary layer over Delhi during autumn and winter months, low wind-speeds (1-3 ms^{-1}) and poor ventilation and mixing means air pollutants from the IGP advected towards Delhi remain close to the surface, aiding the build-up of pollutants. Previous studies have found that ~40% of black carbon loadings in Delhi originate from crop residue and other biomass burning sources in October and November (e.g. Bikkina et al., 2019; Kanawade et al., 2020).

85
Delhi is one of the world's largest cities, with a population exceeding 11 million (Census of India. 2011), experiencing some of the poorest air quality in the world (Pandey et al., 2021). A rapid population growth coinciding with the ever-expanding transportation and city infrastructure has made Delhi one of the most polluted megacities in India (Singh et al., 2021), and indeed the world (Kumar et al., 2017; Hama et al.,
90 2020), suffering ~10k cases of premature mortality per year caused by air pollution (Chen et al., 2020). Winter air pollutant concentrations are particularly high, with daily mean particulate matter with a diameter less than 2.5 micrometres (PM$_{2.5}$) concentrations of 100-200 µg m^{-3} (Singh et al., 2021), peaking at over 1000 µg m^{-3} (Bikkina et al., 2019). As a result of the high pollution levels in Delhi several policies have been implemented over the past few decades (Guttikunda et al. (2023)). For example, an odd-even
95 traffic intervention was brought in during winter and summer in 2016, allowing only odd and even number plates to be used on alternate days. However, analysis of surface observational data did not show any clear concentration reduction in PM$_{2.5}$ (Kumar et al., 2017) highlighting one of the key challenges in this

region: a lack of understanding surrounding the impacts of emissions from the wider region on air quality
in Delhi, which prevents effective policy implementation.

100

Several previous studies have used back-trajectories and chemical transport models to link high pollutant
concentrations in selected cities to the arrival of air masses which had passed over high emission regions
(Reddington et al., 2014; dos Santos et al., 2021; Wehner et al., 2008). Reddington *et al.* (2014) found
that during high pollution episodes, linked with biomass burning, increased concentrations of related
105 tracer species (e.g. levoglucosan) were observed (Atwood et al., 2013; Engling et al., 2014). Similarly,
back-trajectory methods and weather typing have also been applied to assess the contribution of local
emissions and long-range transport to regional and city-level air pollution in many European regions
(Graham et al., 2020; Pope et al., 2016, 2014; Stirling et al., 2020). For example, Pope *et al.* (2014)
sampled satellite NO_2 under different synoptic weather patterns (Lamb weather types, LWTs) to show
110 that UK NO_2 is generally increased under winter-time anti-cyclonic conditions through pollutant
accumulation. NO_2 was also enhanced under south-easterly flow due to long-range transport of pollutants
from continental Europe. The wintertime increase was attributed to the combined effect of increased
emissions, more stable meteorological conditions and decreased photolysis, allowing accumulation over
emission sources. Subsequently Stirling *et al.* (2020) and Graham *et al.* (2020) extended this methodology
115 to analyse changes in NO_x and $PM_{2.5}$ concentrations. They found that long-range transport of NO_x and
$PM_{2.5}$ played a larger role in cities in the south of the UK than the north, with the highest contribution
from long-range transport under easterly, south-easterly, and southerly flows.

Here our approach is similar to Stirling *et al.* (2020) and Graham *et al.* (2020). We combine satellite
120 tropospheric column NO_2 ($TCNO_2$) (top-down) and anthropogenic and fire emissions of NO_x (bottom-
up) with back-trajectories released from Delhi during 2017 and 2018. We aim to quantify the contribution
of local and non-local emissions sources under different seasons and wind directions. Studies such as this
have proved useful elsewhere in the world (e.g. Grundström et al., 2015, 2017; Pope et al., 2014, 2016;
Tang et al., 2009), identifying source sectors and air masses contributing to air pollution and allowing for
125 targeted emissions reductions. However, there have been very few source contribution studies in India.
We then go on to identify key source sectors contributing to poor NO_x AQ in Delhi by individually
excluding sectors from the bottom-up anthropogenic emissions dataset. Section 2 describes the datasets
and method used, Section 3 presents our results and Section 4 summarises the implications of our findings.

130

2. Methods

2.1. Anthropogenic NO_x emissions

2.1.1. Delhi Emissions

We created a merged emissions dataset containing both anthropogenic and daily fire emissions (Figure
135 1f). Anthropogenic NO_x emissions for Delhi are taken from the 2018 System of Air Quality and Weather
Forecasting And Research (SAFAR) dataset (Beig, 2018) (Figure 1a). Data for the SAFAR emission
inventory were collected during a 37,500-hour campaign and is provided at very high (400 m) resolution
over a region covering 70 km × 65 km. Emissions are provided for 26 different source sectors. Emissions
are very detailed, for example emissions for transport were calculated using traffic volume collected by
140 click counters across the region. Collected data was then converted into emissions using a Geographical
Information System (GIS)-based statistical model. Since SAFAR provides a much more detailed, and up-
to-date, inventory of emissions in Delhi we replace EDGAR-HTAP2 Delhi emissions (see 2.1.2 for more
details) with SAFAR emissions, which we regrid from 400 m to 10 km resolution.

145 #### 2.1.2. Global Emissions

We combine Delhi-specific NO_x emissions from SAFAR with global NO_x emissions from the Emission Database for Global Atmospheric Research with Task Force on Hemispheric Transport of Air Pollution (EDGAR-HTAP2) 2010 dataset (Janssens-Maenhout et al., 2015), which are at 10 km resolution (Figure 1c). A comparison between emissions over Delhi from the SAFAR and EDGAR-HTAP2 emissions datasets is also shown in Figure 1a and 1b. This clearly demonstrates the SAFAR dataset provides more spatial detail than EDGAR-HTAP2. EDGAR-HTAP2 is a global, gridded, air pollution emission inventory compiled using officially reported, national gridded inventories; if national emissions datasets for specific sectors were not available EDGAR v4.3 grid maps are used. The resulting EDGAR-HTAP2 dataset provides monthly and annual emission distribution along with emission factors that are fuel-, technology-, process- and human activity-dependent. Emissions include all anthropogenic emissions except large-scale biomass burning (e.g. wildfires).

2.1.3. Fire Emissions

Wildfire NO_x emissions for 2018 are taken from the Fire Inventory from NCAR (FINNv2.5) dataset (Wiedinmyer et al., 2011) at 10 km resolution (Figure 1e) and merged with the anthropogenic emissions dataset (to generate Figure 1f). FINNv2.5 combines data from the Moderate Resolution Imaging Spectroradiometer (MODIS) sensors on NASA's Terra and Aqua satellites with Visible Infrared Imaging Radiometer Suite (VIIRS) on Suomi NPP. We chose to use FINNv2.5 because of its improved ability to detect small, low temperature fires which are likely to be important in India (e.g. agricultural burning). Both MODIS and VIIRS use a Thermal Anomalies Product to provide detections of active fires. MODIS detections are provided at 1 km resolution, while VIIRS has a resolution of 375 m. In FINN, fire hotspot detections from MODIS and VIIRS are combined with land cover, biomass consumption estimates and emissions factors to calculate daily fire emissions globally at 1 km resolution. Burned area is assumed to be 1 km^2 or 0.14 km^2 for each fire identified by MODIS or VIIRS, respectively, and scaled back based on the density of vegetation from the MODIS Vegetation Continuous Fields (VCF) (i.e. if 50% bare = 0.5 km^2 or 0.07 km^2 burned area). The type of vegetation burned during a detected fire is determined using the MODIS Collection 5 Land Cover Type (LCT). Each fire pixel is assigned to one of 16 possible land cover/land use. The 16 land cover types are then aggregated into eight generic categories to which fuel loadings are applied (Wiedinmyer et al., 2011). Fuel loadings are from Hoelzemann *et al.* (2004) and emissions factors are from Akagi *et al.* (2011), McMeeking (2008) and Andrae and Merlet (2001). FINN includes all emissions from above-ground vegetation but not from the combustion of peat (Kiely et al., 2019). Fire types included are wildfires, prescribed and agricultural burning. However, trash-burning or biofuel use are not included.

The merged emission dataset described above provides the control scenario in which all sectors are included (Figure 1f). Additionally, a further 6 emissions files were generated where individual sectors are excluded (transport, industry, power, residential, other and fires) to quantify their contribution to accumulated NO_x along the trajectory path.

2.2. Satellite data

We use tropospheric column nitrogen dioxide (TCNO$_2$) measurements for February 2018 to January 2020 from the TROPOMI instrument on-board ESA's Sentinel-5 Precursor (S5P) satellite that was launched on 13th October 2017. TROPOMI is a hyper-spectral nadir-viewing imager with an equator overpass time at ascending node of 13:30. The NO_2 columns are derived using TROPOMI's UVIS spectrometer backscattered solar radiation measurements in the 405–465 nm wavelength range (van Geffen et al., 2015, 2019). The swath is divided into 450 individual measurement pixels, which results in a near-nadir resolution of 7.0 km × 3.5 km. The total NO_2 slant column density is retrieved from the Level 1b UVIS radiance and solar irradiance spectra using Differential Optical Absorption Spectroscopy (van Geffen et al. 2019). Tropospheric and stratospheric slant column densities are separated from the total slant column using a data assimilation system based on the TM5-MP chemical transport model, after which they are converted into vertical column densities using a look-up table of altitude-dependent air-mass factors. As

data was available from February 2018 onwards, we selected the two years (2018-2019) closest to the back-trajectories (2017-2018) and anthropogenic (2010/2018) and fire emissions (2018) for our analysis. We follow the approach of Pope *et al.* (2018) to map TROPOMI TCNO₂ data onto a 0.05° × 0.05° grid over India.

2.3. Back Trajectories

Our approach is to combine back trajectories with either top-down satellite TCNO₂ or bottom-up NOₓ emission estimates to investigate the influence of long-range transport (advection) of NOₓ on ambient concentrations under different wind-directions in Delhi. In the following section we will refer to bottom-up NOₓ emissions, however the method is the same when using satellite TCNO₂.

We use primary NOₓ emissions integrated over air mass back-trajectories to determine the relative influence of direct NOₓ emissions on those air masses. Back-trajectories are calculated using the Reading Offline TRAJectory (ROTRAJ) Lagrangian transport model (Methven, 2003). The model uses dynamical fields from ERA-Interim reanalysis from the European Centre for Medium-Range Weather Forecasts (ECMWF) to calculate trajectories at 1.125° horizontal resolution. After a trajectory parcel is released, its location is calculated every 6 hours; for vertical interpolation the model uses cubic Lagrangian interpolation and horizontal fields are calculated using bilinear interpolation. This approach primarily focuses on large-scale advection and does not resolve small-scale sub-grid turbulent transport or convection.

In this study, ROTRAJ back trajectories were released from just above the surface (0.99 sigma level; a terrain following coordinate system where 1 is the surface) in central Delhi at 06:00 UTC (11:30 local time) for the years 2017 and 2018, extending back 4 days in 6-hour time steps. We choose 06:00 UTC (11:30 local time) as this is close to mid-day local time and so matches the time of the satellite overpass time (13:30 local time) most closely. We are restricted to using ROTRAJ back-trajectories for 2017 and 2018, while using satellite data for 2018 and 2019, as the ECMWF ERA-Interim reanalysis dataset was terminated in August 2019 and satellite data is not available until 2018. NOₓ emissions were accumulated along each trajectory over 4 days at 15-minute time intervals (interpolated linearly from 6-hourly position output) (Figure 2).

NOₓ emissions were only accumulated only if the trajectory path was within the boundary layer (based on ERA-Interim). At each location, we accumulate the entire emission within an emission grid box (TCNO₂: ~5 km, emissions: ~10 km) over which the trajectory passes. The surface area of each grid box that the trajectory points passed over is also accumulated over time.

The along-trajectory emission accumulation can be represented by Equation (1):

$$E_i = [E_{i-1} + \emptyset_i . \Delta t . \alpha_i] e^{-\Delta t / \tau_i} \tag{1}$$

where i=1,N (=384) and E_0 =0.0

E_i is accumulated NOₓ (kg) at any given point i along the trajectory, ϕ_i is the emissions flux of NOₓ (kg m⁻² s⁻¹) at point i, Δt is the 15-minute time step, α is the surface area of the grid box (m²) at point i and τ_i is the specified NOₓ lifetime (τ) at point i. Therefore, E_N is total accumulated NOₓ mass (kg) and N is the number of 15-minute time steps within the 4-day trajectory (384).

To account for chemical loss of NO_x along the trajectory path, the lifetime of NO_2 was calculated at each timestep from TOMCAT (Chipperfield, 2006; Monks et al., 2017) 3-D hourly hydroxyl radical (OH), pressure and temperature fields, assuming the main loss pathway in Equation (2), where NO_2 is oxidised by OH to form nitric acid (HNO_3) (which dominates over photolysis within the boundary layer). The NO_x lifetime (τ) (Equation (3)) was calculated using a temperature and pressure-dependent rate constant (k) (IUPAC, 2022). The calculated lifetime (τ) was then applied to the total NO_x accumulated emission in the air parcel in Equation (1).

$$OH + NO_2 + M \rightarrow HNO_3 + M \tag{2}$$
$$\tau = 1/(k.[OH]) \tag{3}$$

To remove the dependence of the accumulated emissions calculated in Equation (1) on emission grid resolution (since we assumed the air mass has the same width as the emission grid box), the total accumulated NO_x mass (E) was divided by accumulated surface area (S) and then scaled by 10^9 to give E units of $\mu g\ m^{-2}$. S is given by Equation (4):

$$S = \sum_{i=1}^{N} a_i \tag{4}$$

Emissions accumulated within Delhi (*EDelhi*) were also determined using the same approach, but only implemented when the trajectories enter the Delhi region, which we define using a bounding box (76.8 - 77.5°E, 28.1 - 28.9°N). To derive *EDelhi* in units of $\mu g\ m^{-2}$, the accumulated NO_x mass from Delhi was divided by the accumulated surface area (S) over the full trajectory path. The ratio between *EDelhi/E* represents the fractional contribution of Delhi sources towards the total accumulated NO_x emissions.

Finally, the daily (06:00 UTC) total accumulated emission and *EDelhi/E* ratios from all sites were binned by the wind direction. This methodology provides a powerful tool to identify which flow directions are the most polluted and to derive the proportion of pollutant emissions from long-range transport versus local sources.

2.4 Observational Data

The hourly averaged surface NO_2 concentration at 36 sites over Delhi for 2018 and 2019 (Figure 3) were obtained from the CAAQMS (Continuous Ambient Air Quality Monitoring Stations) portal (https://app.cpcbccr.com/ccr/#/caaqm-dashboard-all/caaqm-landing) of the Central Pollution Control Board (CPCB) of India. The ambient NO_2 concentration was measured based on the Gas Phase Chemiluminescence methodology; the technical details of monitoring can be found in CPCB (2019). The data was further quality controlled to remove outliers and missing values (Singh et al., 2020). As TROPOMI has a local overpass time of approximately 13:30, the average NO_2 between 13-14 hours was calculated for each site to represent the daily NO_2 corresponding to the overpass of TROPOMI. From this, the daily median NO_2 concentration across all sites was calculated to represent daily NO_2 levels over Delhi in 2018 and 2019.

3. Results

The contribution of local and non-local sources to NO_2 levels in Delhi are controlled by primary emissions, the chemical lifetime of NO_2 and advection by meteorology (i.e. accumulation/advection of

pollutants under stable conditions or ventilation of source emissions downwind). Figure 4b, c and d show the annual average $TCNO_2$, surface NO_2 lifetime and boundary layer height (BLH) over India along with the anomalies for the pre-monsoon (February - April), monsoon (May - September) and post-monsoon (October - January) seasons.

290

Peak annual $TCNO_2$ ranges between 4000 and 5000 µg m^{-2} over the source regions (e.g. Delhi, Kolkata, Nagpur and industrial sources in the east (approximately 80-85°E, 20-25°N)) (Figure 4b). Smaller urban NO_2 hotspots range between 3000 and 4000 µg m^{-2}. In the seasonal anomaly, the pre-monsoon $TCNO_2$ values increase by approximately 500-1000 µg m^{-2} around Delhi but with similar decreases to the north-

295 west. However, the majority of the country experiences $TCNO_2$ increases greater than 2000 µg m^{-2}. During the monsoon season there is a decrease in $TCNO_2$ by 1000-1500 µg m^{-2} over Delhi, which is reflected in the majority of other urban centres and industrial regions. The post-monsoon season experiences the largest degradation in NO_2-related air quality as all hotspots increase by >2000 µg m^{-2} (e.g. for Delhi) with peak enhancements over the industrialised region in the east of India.

300

The calculated NO_2 lifetime (based on modelled OH, temperature and pressure) typically ranges between 1.5 to 15 hours over India (between 20 and 24 hours over Bangladesh and Myanmar) and 8 to 12 hours over Delhi (Figure 4c). During the pre-monsoon, there is little change from the annual average, decreasing by 1 to 2 hours over Delhi. Along the Indian east coastline, there is a general decrease of 3-5 hours. During

305 the monsoon season, there are large reductions in the NO_2 lifetime over the northern segment of the domain, decreasing by 5 to 10 hours, propagating southwards to Delhi with a decrease of approximately 3-5 hours. Central India remains similar to the annual average while the east coastline now experiences increases in the NO_2 lifetime of 3 to 5 hours. In the post-monsoon, while southern India experiences little change, Delhi and the north of India see an increase in the lifetime by 3-7 hours.

310

Western India has an annual average BLH ranging between 800 and 1100 m (400-800 m over eastern India), while Delhi BLH is between 400 and 600 m (Figure 4d). In the pre-monsoon, the Indian boundary layer is well ventilated with an increase in BLH by ~200 to 400 m (50-100 m for Delhi). In the monsoon season, the boundary layer remains well ventilated with enhancements of typically 100 to 200 m (although

315 with some regions of reduction in the BLH), relative to the annual average. In the post-monsoon season, colder temperatures cause country-wide shallowing of the boundary layer by 200 to 400 m, including Delhi, peaking at over 500 m in central India.

The pre-monsoon and, especially, post-monsoon season conditions are favourable for the degradation in

320 NO_2 air quality given the typically larger primary NO_x emissions (e.g. from increased domestic heating and power demands), the longer NO_2 lifetime (i.e. less chemical loss) and shallower boundary layer trapping emissions over Delhi and the wider IGP. In contrast, the lower emissions, shorter NO_2 lifetime and atmospheric ventilation of the boundary layer yield lower pollution levels during the monsoon season. We have thus demonstrated the seasonal influences on NO_2 levels in Delhi and surrounding region but

325 now exploit the back-trajectory integrated emissions methodology (see Section 2) to determine the balance of local versus non-local sources of NO_x to Delhi air quality. Here, we accumulate $TCNO_2$ from TROPOMI under the back trajectories to investigate the seasonal influence of wind direction on the advection of $TCNO_2$ into Delhi. As discussed above, there is a clear seasonal influence of the monsoon circulation on the back-trajectories integrated emission totals.

330

On average, the back-trajectories arrive into Dehli at the surface from the south-west, east and north-west (Figure 4a). Trajectories from the south-west have the lowest accumulated $TCNO_2$ levels (0-200 µg m^{-2}), largely originating over the Arabian Sea (i.e. fewer NO_x sources) before arriving in Delhi. Trajectories originating from eastern India pass over several large urban centres and industrial regions yielding

335 integrated $TCNO_2$ trajectories with $TCNO_2$ levels that range between 400 to 700 µg m^{-2} before arriving in Delhi. The trajectories from the north-west are the most polluted, with peak $TCNO_2$ levels of >1000 µg m^{-2}. When split seasonally, the pre-monsoon shows trajectories approaching Delhi from the north-west (200-400 µg m^{-2}) and east (600-900 µg m^{-2}). In the monsoon, cleaner airmasses (0-200 µg m^{-2}) originate from the south-west while eastern airmasses remain similarly polluted as the pre-monsoon (600-

340   800 µg m^{-2}). During the post-monsoon, most trajectories are from the north-west of India and show the largest seasonal pollution levels (i.e. integrated TCNO$_2$ back-trajectories of typically 800 to >1000 µg m^{-2}).

We repeated this approach using the bottom-up emissions inventory (Figure 5) with close agreement to
345   the TCNO$_2$ results. In the pre-monsoon season, the integrated emission back-trajectories range between 80 and 120 µg m^{-2} from both the east and north-west. Note the emission trajectory values are lower than the equivalent TCNO$_2$ values as they are emission fluxes and not the tropospheric integrated column. In terms of altitude, the trajectories range from the near-surface to 400 hPa. At t=96 hours before arrival at Delhi, the median trajectory position is near 800 hPa before descending below 950 hPa at approximately
350   30 hours from Delhi. In the vertical distribution, there is no clear link between the integrated emission trajectory values and altitude. During the monsoon season, there are two limbs of integrated emission trajectories with TCNO$_2$ ranging between 0 and 40 µg m^{-2} from the south-west and 40-80 µg m^{-2} from the east. The average trajectory position is lower in altitude, starting at approximately 950 hPa and remaining below this pressure level. There appears to be a split in the trajectory origins and altitudes with
355   south-western trajectories coming from the Arabian Sea near the surface with few emissions sources (airmasses will be influenced to some extent by shipping emissions but the short NO$_2$ lifetime will yield limited impact in Delhi), while more polluted trajectories (i.e. substantial upwind sources) from the east are typically 900-600 hPa in altitude. During the post-monsoon season, the median trajectory altitude is approximately 875 hPa at 96 hours upwind of Delhi. For the final 24 hours or so, the trajectories converge
360   on Delhi below 950 hPa. As a result, while all seasons experience trajectories 1-day out from Delhi below 950 hPa, the post-monsoon trajectories are closer to the surface than the pre-monsoon equivalent throughout the 4 days and are exposed to larger emission fluxes than those during the monsoon. Secondly, as these post-monsoon trajectories originate from the north-west and are trapped in the IGP by the Himalayas, there is the opportunity for re-circulation of the trajectory over up-wind NO$_x$ sources. Overall,
365   the meteorological, chemical and emission factors yield, all trapped against the Himalayas, in the post-monsoon season, are key for the substantial degradation in the air quality.

The integrated emission trajectories also provide the opportunity to gain better insight about the proportion of local vs. non-local sources (i.e. integrated trajectories over the full 4 days vs. integrated
370   trajectories just over Delhi). Figure 6 shows this but note we only plot wind directions where the sample size is greater than or equal to 10. We find that during the pre-monsoon season, the grouped integrated emissions trajectories are moderately polluted (south-west, west, north-west and north range between 10 and 50 µg m^{-2}) with a peak average easterly value of approximately 65 µg m^{-2}. In terms of local contributions, east, north and south-westerly flows are dominated by local sources (i.e. >60%).
375   Trajectories from the west and north-west are dominated by non-local sources (i.e. <40% local) but the absolute values of the integrated back trajectories are relatively smaller with limited impact on Delhi AQ. During the monsoon, all the wind directions (easterly, south-easterly, south-westerly, westerly and north-westerly) have lower integrated emission back-trajectories (integrated NO$_x$ emissions peaking at approximately 40 µg m^{-2}) with over 80% of emissions coming from local sources. For poor air quality,
380   as discussed above, the post-monsoon season is the most important as integrated emission trajectory values from the north (sample size = 17), north-west (179), north-east (10) and east (21) range between 60 and >100 µg m^{-2} on average. Despite the larger integrated emissions trajectory median values, the key factor is the local contribution only ranging between 30 and 65%. The north-westerly trajectory value is the largest and most frequent (i.e. 73% of trajectories originate from the north-west) during the post-
385   monsoon season with approximately 70% of emission contributions coming from outside of Delhi. Thus, we find that the dominating advection of highly polluted air originating from outside Delhi is the primary contributor to the Delhi population and air quality mitigation strategies need to be adopted not only in Delhi but also in the surrounding regions to successfully control this issue.

390   Next, we quantify the influence of individual sectoral emissions to the total accumulated emissions by running the back trajectory analysis without individual emissions source sectors and analysing accumulated emissions (Figure 7, note that only wind-directions with a sample size greater than or equal to 10 are shown). During the pre-monsoon season, accumulated emissions from transport are the dominant

contributor (>50%) and non-local sources are most important (60-80%) under the most frequent north-
westerly and westerly wind directions. Trajectories travel close to the surface, within the boundary layer,
in the final 24 hours and the NO_x lifetime is short. This indicates that a large fraction of the total integrated
emissions reaching Delhi are likely to have originated in the region surrounding the city, where the NO_x
burden from transport is high. Additionally, the contribution of non-local industrial and residential
emissions is evident. This is likely because there are few large coal-fired power stations located to the
north-west of Delhi in Punjab and Haryana. There is also a strong reliance on open stoves and fires for
cooking and heating in nearby states such as Uttar Pradesh.

During the monsoon season, easterly (easterly and south-easterly) and westerly (south-westerly and north-
westerly) winds dominate. Under all directions local accumulated emissions show nearly similar
contribution (50-90%) for all sectors. Although many trajectories travel from distant regions, remaining
close to the surface, there are few sources over the ocean (apart from shipping) and the NO_x lifetime is
short, so the advection of accumulated emissions concentration is much lower. Therefore, the small
contribution of non-local sources is likely from nearby regions within the polluted IGP. Overall, transport
emissions have the highest contribution to overall accumulated emissions (>40%), which is likely driven
by transport emissions dominating the NO_x burden in Delhi. In addition, contributions from local power
and industrial emissions are also important under easterly and south-easterly (and north-westerly) wind
directions with only a small non-local contribution to the overall emissions (10-20%) and are likely to
originate from the large industrial region to the east of Delhi and from power generation to the north-
west.

During the post-monsoon winds are primarily north-westerly and are associated with high contributions
from transport emissions (70% non-local emissions), with non-negligible contributions from industry,
other, power and residential emissions (and negligible contributions from fires). Again, non-local sources
generally dominate for these sectors (up to 100%) with the largest probable contribution from within the
IGP region surrounding Delhi where residential emissions are high. The large contribution of non-local
emissions in all sectors is likely driven by the combination of several factors. First, a longer NO_x lifetime,
arising from OH being less abundant (to react with NO_x) that enables accumulated emissions to be
advected over long (and short) distances from high emission regions north-west of Delhi. Second, a
shallow boundary layer that traps emissions close to the surface, allowing them to accumulate. Third, an
increase in emissions during winter months due to increased demand for heating (residential sector) and
power (power sector).

Finally, we apply the same back-trajectory emissions method to the high pollution days in Delhi to
investigate the drivers of high-pollution events in the city. We use daily median ground-based NO_2
observations from sites in Delhi to identify high pollution days, defined as days where daily median NO_2
concentrations are above the 90th percentile of daily median NO_2 concentrations (>37 µg m^{-3}) between 1st
January 2017 and 31st December 2018 (Figure 8a). We then subsample the trajectories using these high
pollution days and attribute the accumulated emissions to specific emissions sectors.

There is a clear seasonal cycle in NO_2 concentrations in Delhi, with maximum NO_2 values occurring
during pre- and post-monsoon months that peak in December (up to ~60 µg m^{-3}), and minima during
monsoon months (20 to ~30 µg m^{-3}) (Figure 8a). We also find that BLH is inversely related with median
NO_2 concentrations, indicating a shallow boundary layer (<600 m) during the pre- and post-monsoon and
a higher boundary layer (600-1500 m) during the monsoon (Figure 8b). Additionally, the atmospheric
lifetime of NO_x is highest in pre- and post-monsoon months (>10-70 hours) and is lowest during the
monsoon season (~10 hours (Figure 8c). Finally, NO_x emissions are also highest during the pre- and post-
monsoon (~0.05-0.07 kg m^{-2} s^{-1}) and lowest during the monsoon season (<0.055 kg m^{-2} s^{-1} Figure 8d).
The combination of these factors aids the accumulation of increased local emissions during the pre- and
post-monsoon months and the dispersal of the decreased emissions during the monsoon. Thus, the non-
monsoon seasons, especially in the post-monsoon, experience a substantial degradation in air quality.

The back trajectory emissions analysis indicates that high-pollution days are associated with trajectories from the north-west of Delhi (Figure 9a) in both the pre- (n=12 days) and post-monsoon (n=60 days). Note that we only include wind-directions with a sample size greater than or equal to 5 (easterly and north-westerly). Trajectories gradually descend towards the surface between 90 and 20 hours out from Delhi, remaining close to the surface (>950 hPa) until they reach Delhi (Figure 9b). However, during the post-monsoon trajectories are much closer to the surface from hour 90 (910-810 hPa) compared with the pre-monsoon (840-770 hPa), likely allowing increased accumulation of emissions. During post-monsoon high-pollution days non-local (>80% non-local) transport emissions dominate (>75%) the total accumulated emissions (Figure 10). This is likely due to the trajectories remaining close to the surface for the final 24 hours, within a shallow boundary layer, at a period when the NO_x atmospheric lifetime and emissions are increased. The contribution of other sectors to the remaining accumulated emissions (residential, industrial, other and power) is smaller but non-local emissions remain important (25-100%). There is also a negligible contribution (<2 µg m^{-3}) from non-local (100%) fires under north-westerly winds. Overall, this suggests that non-local emissions from long-range transport (advection) are important during episodes of very poor AQ in Delhi.

4. Discussion and Conclusions

4.1 Seasonal wind flow regimes

In this study we have used high-resolution satellite tropospheric column NO_2 ($TCNO_2$) data from TROPOMI and bottom-up NO_x emission inventories alongside a back-trajectory model to investigate the influence of local and the advection of pollutants to Delhi throughout the year. We also performed sensitivity simulations to separate the influence of various sectoral emissions on the accumulated pollution, by removing individual emission source sectors. We summarise our findings in Table 1, which gives the dominant wind-direction(s) in each season as a percentage of days in the season, the source sectors with the largest contribution to the accumulated emissions under that wind direction and finally, the contribution of local (Delhi) or non-local (rest of India) accumulated emissions to the total accumulated emissions. Our analysis indicates that emissions accumulated over 4 days are highest under easterly, northerly and north-westerly directions during the pre- (~60-90 µg m^{-2}) and post- (~70-110 µg m^{-2}) monsoon months. During the pre-monsoon season, north-westerly wind directions dominate (54%) and transport emissions account for 80% of the total accumulated emissions, with non-local emissions contributing ~70% of the total transport accumulated emissions. The high accumulated emissions observed under these wind directions are likely driven by high local NO_x emissions during the pre-monsoon (since NO_x lifetime is relatively short and the boundary layer is relatively deep). During the post-monsoon, north-westerly wind dominates (73%) and transport emissions (73%), which are non-local (70%), are most important. During this period high emissions are accompanied by a longer NO_x atmospheric lifetime and shallow boundary-layer, aiding the build-up of emissions along the trajectory path and leading to increased contribution from the advection of NO_x into the city under north-westerly flow. In addition, non-local (50-100%) residential, power and industrial emissions also contribute to the total accumulated emissions under north-westerly winds during the post-monsoon. Emissions are likely due to increased demand for heating and power during the colder post-monsoon months, particularly in Punjab and Haryana, where there are few large coal-fired power stations, and nearby states, such as Uttar Pradesh, where there is a strong reliance on open stoves and fires for cooking and heating.

4.2 Source attribution during high pollution episodes

We also applied the back-trajectory method to high-pollution days, defined as days where median NO_2 concentrations (from ground-based observations) are above the 90th percentile. The ground-based observations indicate that high-pollution episodes are most common in the post-monsoon (>80% of occurrences) and are dominated by days where winds were from the north-west (>75%). On these days (north-westerly winds during the post-monsoon) non-local (>80%) transport emissions dominate (>75%). The large contribution of non-local transport emissions is likely driven by trajectories (air masses) that

travel towards Delhi remaining close to the surface, accumulating increased emissions that are not quickly lost due to decreased sunlight and therefore less abundant OH during winter months. The small contribution (20%) of local transport emissions is likely driven by high NO_x emissions in a shallow boundary layer, which acts to traps pollutants at the surface.

505

The results of this study are in line with previous work by Sembhi *et al.* (2020) who used a model to simulate air quality in Delhi during a poor AQ episode in 2016 with and without the implementation of the SSWA. They found that timing shift in agricultural burning in north-west India caused by the introduction of the SSWA contributed only around 3% to the poor AQ observed, indicating that this was largely driven by other factors. We also find that trajectories originating from the north-west during post-510 monsoon months have a polluted footprint in both the satellite and emissions analysis. However, within our work we do not see an impact from the advection of NO_x fire emissions, which could be for a number of reasons. Firstly, Sembhi *et al* (2020) focussed on $PM_{2.5}$, which has a much longer atmospheric-lifetime than NO_x (days to weeks compared with hours to days). This leads to a smaller contribution in the 515 advection of NO_x from fires occurring in north-west India during the post-monsoon. In addition, fire emissions are generated using polar orbiting satellites which have a single daytime overpass and thus may miss fires which have a short burn time; fire emissions inventories currently struggle to detect agricultural waste burning fires due to their small size and often short burn times (Zhang et al., 2020; Liu et al., 2020). Although we have used VIIRS in this study (which is able to detect smaller, lower temperature fires than 520 MODIS) the total emissions from agricultural waste burning may still be underestimated (Zhang et al., 2020; Liu et al., 2020). With the introduction of geostationary satellites and sensors which can continuously detect smaller fires (e.g. Himawari) it should be easier to constrain the emissions from agricultural waste burning in the future. However, this work provides further evidence that the advection of non-local pollutants to Delhi plays an important role in both ambient and high pollution conditions, in 525 line with Sembhi *et al.* (2020).

4.3 Implications for policy to control air pollution over Delhi

Transport emissions dominate under all wind-directions and seasons indicating that emissions reductions 530 in this sector would lead to the largest benefits. However, to improve local AQ in Delhi transport emissions would need to be reduced both locally and regionally. This is particularly important for high pollution events where non-local transport emissions dominate.

Code Availability
535
Code used to generate the figures in this paper is available on request.

Data Availability

540 Data used in this paper is available on request.

Author Contributions

AMG processed emissions datasets, adapted and ran back-trajectory code, previously written by RJP, 545 and created all figures. RJP downloaded and processed satellite data. SD downloaded and processed ERA-Interim data. AMG wrote the manuscript with input from RJP, SD and MPC. MP provided TOMCAT 3D OH fields from model simulations which WF helped set-up. VS provided ground-based NO_2 observations from Delhi. YC and OW helped with NO_2 lifetime calculations. RS provided guidance and feedback on the work. GB provided SAFAR NO_x emissions.
550
Competing Interests

The authors declare that they have no conflict of interest.

555 **Acknowledgements**

560

References

565 Ahmed, W., Tan, Q., Ali, S. and Ahmad, N., 2019. Addressing environmental implications of crop stubble burning in Pakistan: innovation platforms as an alternative approach. *International Journal of Global Warming,* **19**(1-2), pp. 76-93. DOI: https://doi.org/10.1504/IJGW.2019.101773.

Andreae, M.O. and Merlet, P., 2001. Emission of trace gases and aerosols from biomass burning. *Global biogeochemical cycles*, **15**(4), pp. 955-966. DOI:
570 https://doi.org/10.1029/2000GB001382.

Akagi, S.K., Yokelson, R.J., Wiedinmyer, C., Alvarado, M.J., Reid, J.S., Karl, T., Crounse, J.D. and Wennberg, P.O., 2011. Emission factors for open and domestic biomass burning for use in atmospheric models. *Atmospheric Chemistry and Physics*, **11**(9), pp. 4039-4072. DOI: https://doi.org/10.5194/acp-
575 11-4039-2011.

Atwood, S.A., Reid, J.S., Kreidenweis, S.M., Liya, E.Y., Salinas, S.V., Chew, B.N. and Balasubramanian, R., 2013. Analysis of source regions for smoke events in Singapore for the 2009 El Nino burning season. *Atmospheric Environment*, **78,** pp. 219-230. DOI:
580 https://doi.org/10.1016/j.atmosenv.2013.04.047.

Badarinath, K.V.S., Kharol, S.K., Sharma, A.R. and Prasad, V.K., 2009. Analysis of aerosol and carbon monoxide characteristics over Arabian Sea during crop residue burning period in the Indo-Gangetic Plains using multi-satellite remote sensing datasets. *Journal of Atmospheric and Solar-Terrestrial*
585 *Physics,* **71**(12), pp. 1267-1276. DOI: https://doi.org/10.1016/j.jastp.2009.04.004.

Beig, G., Sahu, S.K., Dhote, M., Tikle, S., Mangaraj, P., Mandal, A., Dhole, S., Dash, S., Korhale, N., Rathod, A. and Pawar, P., 2018. SAFAR-high resolution emission inventory of Megacity Delhi for 2018. *Special Scientific Report, SAFAR-Delhi-2018-A, ISSN*, pp. 0252-1075.
590

Bikkina, S., Andersson, A., Kirillova, E.N., Holmstrand, H., Tiwari, S., Srivastava, A.K., Bisht, D.S. and Gustafsson, Ö., 2019. Air quality in megacity Delhi affected by countryside biomass burning. *Nature Sustainability*, **2**(3), pp. 200-205. DOI: https://doi.org/10.1038/s41893-019-0219-0.

595 Central Pollution Control Board (CPCB), 2019. Central Control Room for Air Quality Management - All India. Available at: https://app.cpcbccr.com/ccr/#/caaqm-dashboard-all/caaqm-landing

Census of India. 2011. *Census of India: Provisional Population Totals Paper 1 of 2011, NCT of Delhi*. [Online]. [Accessed 31 January 2023]. Available from:
600 https://web.archive.org/web/20220119042828/https://censusindia.gov.in/2011-prov-results/prov_data_products_delhi.html

Chen, Y., Wild, O., Conibear, L., Ran, L., He, J., Wang, L. and Wang, Y., 2020. Local characteristics of and exposure to fine particulate matter ($PM_{2.5}$) in four Indian megacities. *Atmospheric Environment: X*,
605 **5,** p. 100052. DOI: https://doi.org/10.1016/j.aeaoa.2019.100052.

Chipperfield, M.P., 2006. New version of the TOMCAT/SLIMCAT off-line chemical transport model: Intercomparison of stratospheric tracer experiments. Quarterly Journal of the Royal Meteorological Society: A journal of the atmospheric sciences, applied meteorology and physical oceanography,
610 **132**(617), pp. 1179-1203. DOI: https://doi.org/10.1256/qj.05.51.

dos Santos, O.N. and Hoinaski, L., 2021. Incorporating gridded concentration data in air pollution back trajectories analysis for source identification. *Atmospheric Research,* **263,** p. 105820. DOI: https://doi.org/10.1016/j.atmosres.2021.105820.

615 Engling, G., He, J., Betha, R. and Balasubramanian, R., 2014. Assessing the regional impact of indonesian biomass burning emissions based on organic molecular tracers and chemical mass balance modeling. *Atmospheric Chemistry and Physics*, **14**(15), pp. 8043-8054. DOI: https://doi.org/10.5194/acp-14-8043-2014.

620 Graham, A.M., Pringle, K.J., Arnold, S.R., Pope, R.J., Vieno, M., Butt, E.W., Conibear, L., Stirling, E.L. and McQuaid, J.B., 2020. Impact of weather types on UK ambient particulate matter concentrations. *Atmospheric Environment: X*, **5,** p. 100061. DOI: https://doi.org/10.1016/j.aeaoa.2019.100061.

625 Grundström, M., Tang, L., Hallquist, M., Nguyen, H., Chen, D., Pleijel, H., 2015. Influence of atmospheric circulation patterns on urban air quality during the winter. *Atmos. Poll. Res.* **6** (2), pp. 278–285. DOI: https://doi.org/10.5094/APR.2015.032.

Grundström, M., Dahl, Å., Ou, T., Chen, D., Pleijel, H., 2017. The relationship between birch pollen, air
630 pollution and weather types and their effect on antihistamine purchase in two Swedish cities. *Aerobiologia*, **33**(4), pp. 457-471. DOI: https://doi.org/10.1007/s10453-017-9478-2.

Guttikunda, S.K. Dammalapati, S.K. Pradhan, G. Krishna, B. Jethva, H.T. Jawahar, P., 2023. What Is Polluting Delhi's Air? A Review from 1990 to 2022. *Sustainability*, **15**, p. 4209. DOI:
635 https://doi.org/10.3390/su15054209.

Hama, S.M., Kumar, P., Harrison, R.M., Bloss, W.J., Khare, M., Mishra, S., Namdeo, A., Sokhi, R., Goodman, P. and Sharma, C., 2020. Four-year assessment of ambient particulate matter and trace gases in the Delhi-NCR region of India. *Sustainable Cities and Society*, **54,** p. 102003. DOI:
640 https://doi.org/10.1016/j.scs.2019.102003.

Hoelzemann, J.J., Schultz, M.G., Brasseur, G.P., Granier, C. and Simon, M., 2004. Global Wildland Fire Emission Model (GWEM): Evaluating the use of global area burnt satellite data. *Journal of Geophysical Research: Atmospheres*, **109**(D14). DOI: https://doi.org/10.1029/2003JD003666.
645
IUPAC (Task Group on Atmospheric Chemical Kinetic Data Evaluation), 2022. Evaluated Kinetic Data. Available at: https://iupac-aeris.ipsl.fr/

Jethva, H.T., Chand, D., Torres, O., Gupta, P., Lyapustin, A. and Patadia, F., 2018. Agricultural burning
650 and air quality over northern India: a synergistic analysis using NASA's A-train satellite data and ground measurements. *Aerosol and Air Quality Research*, **18**, pp. 1756-1773. DOI: https://doi.org/10.4209/aaqr.2017.12.0583
Jethva, H., Torres, O., Field, R.D., Lyapustin, A., Gautam, R. and Kayetha, V., 2019. Connecting crop productivity, residue fires, and air quality over northern India. *Scientific reports*, **9**(1), pp. 1-11. DOI:
655 https://doi.org/10.1038/s41598-019-52799-x.

Kanawade, V.P., Srivastava, A.K., Ram, K., Asmi, E., Vakkari, V., Soni, V.K., Varaprasad, V. and Sarangi, C., 2020. What caused severe air pollution episode of November 2016 in New Delhi? *Atmospheric Environment*, **222,** p. 117125. DOI:
660 https://doi.org/10.1016/j.atmosenv.2019.117125.

Kiely, L., Spracklen, D.V., Wiedinmyer, C., Conibear, L., Reddington, C.L., Archer-Nicholls, S., Lowe, D., Arnold, S.R., Knote, C., Khan, M.F. and Latif, M.T., 2019. New estimate of particulate emissions from Indonesian peat fires in 2015. *Atmospheric Chemistry and Physics*, **19**(17), pp. 11105-11121.
665 DOI: https://doi.org/10.5194/acp-19-11105-2019.

Kumar, P., Gulia, S., Harrison, R.M. and Khare, M., 2017. The influence of odd–even car trial on fine and coarse particles in Delhi. *Environmental Pollution*, 225, pp. 20-30. DOI: https://doi.org/10.1016/j.envpol.2017.03.017.

670

Kumar, P., Sahu, N.C., Ansari, M.A. and Kumar, S., 2021. Climate change and rice production in India: role of ecological and carbon footprint. *Journal of Agribusiness in Developing and Emerging Economies*. DOI: https://doi.org/10.1108/JADEE-06-2021-0152.

675 Liu, T., Mickley, L.J., Marlier, M.E., DeFries, R.S., Khan, M.F., Latif, M.T. and Karambelas, A., 2020. Diagnosing spatial biases and uncertainties in global fire emissions inventories: Indonesia as regional case study. *Remote Sensing of Environment*, **237**, p. 111557. DOI: https://doi.org/10.1016/j.rse.2019.111557.

680 Liu, T., Mickley, L. J., Gautam, R., Singh, M. K., DeFries, R. S., and Marlier, M. E. (2021). Detection of delay in post-monsoon agricultural burning across Punjab, India: Potential drivers and consequences for air quality. *Environ. Res. Lett.* **16**, p. 014014. DOI: https://doi.org/10.1088/1748-9326/abcc28.

McMeeking, G.R., Kreidenweis, S.M., Baker, S., Carrico, C.M., Chow, J.C., Collett Jr, J.L., Hao, 685 W.M., Holden, A.S., Kirchstetter, T.W., Malm, W.C. and Moosmüller, H., 2009. Emissions of trace gases and aerosols during the open combustion of biomass in the laboratory. *Journal of Geophysical Research: Atmospheres*, **114**(D19). DOI: https://doi.org/10.1029/2009JD011836.

Methven, J., Arnold, S.R., O'Connor, F.M., Barjat, H., Dewey, K., Kent, J. and Brough, N., 2003. 690 Estimating photochemically produced ozone throughout a domain using flight data and a Lagrangian model. *Journal of Geophysical Research: Atmospheres*, **108**(D9). DOI: https://doi.org/10.1029/2002JD002955.

Monks, S.A., Arnold, S.R., Hollaway, M.J., Pope, R.J., Wilson, C., Feng, W., Emmerson, K.M., 695 Kerridge, B.J., Latter, B.L., Miles, G.M. and Siddans, R., 2017. The TOMCAT global chemical transport model v1. 6: description of chemical mechanism and model evaluation. *Geoscientific Model Development*, **10**(8), pp. 3025-3057. DOI: https://doi.org/10.5194/gmd-10-3025-2017.

Mor, S., Singh, T., Bishnoi, N.R., Bhukal, S. and Ravindra, K., 2022. Understanding seasonal variation 700 in ambient air quality and its relationship with crop residue burning activities in an agrarian state of India. *Environmental Science and Pollution Research*, **29**(3), pp. 4145-4158. DOI: https://doi.org/10.1007/s11356-021-15631-6.

Pandey, A., Brauer, M., Cropper, M.L., Balakrishnan, K., Mathur, P., Dey, S., Turkgulu, B., Kumar, 705 G.A., Khare, M., Beig, G. and Gupta, T., 2021. Health and economic impact of air pollution in the states of India: the Global Burden of Disease Study 2019. *The Lancet Planetary Health*, **5**(1), pp. 25-38. DOI: https://doi.org/10.1016/S2542-5196(20)30298-9.

Pope, R.J., Savage, N.H., Chipperfield, M.P., Arnold, S.R. and Osborn, T.J., 2014. The influence of 710 synoptic weather regimes on UK air quality: analysis of satellite column NO_2. *Atmospheric Science Letters*, **15**(3), pp. 211-217. DOI: https://doi.org/10.1002/asl2.492.

Pope, R.J., Butt, E.W., Chipperfield, M.P., Doherty, R.M., Fenech, S., Schmidt, A., Arnold, S.R. and Savage, N.H., 2016. The impact of synoptic weather on UK surface ozone and implications for 715 premature mortality. *Environmental Research Letters*, **11**(12), p. 124004. DOI: https//doi.org/ 10.1088/1748-9326/11/12/124004.

Pope, R.J., Arnold, S.R., Chipperfield, M.P., Latter, B.G., Siddans, R. and Kerridge, B.J., 2018. Widespread changes in UK air quality observed from space. *Atmospheric Science Letters*, **19**(5), p. 817. 720 DOI: https://doi.org/10.1002/asl.817.

Reddington, C.L., Yoshioka, M., Balasubramanian, R., Ridley, D., Toh, Y.Y., Arnold, S.R. and Spracklen, D.V., 2014. Contribution of vegetation and peat fires to particulate air pollution in Southeast Asia. *Environmental Research Letters*, **9**(9), p. 094006. DOI: https://doi.org/10.1088/1748-9326/9/9/094006.

Sembhi, H., Wooster, M., Zhang, T., Sharma, S., Singh, N., Agarwal, S., Boesch, H., Gupta, S., Misra, A., Tripathi, S.N. and Mor, S., 2020. Post-monsoon air quality degradation across Northern India: assessing the impact of policy-related shifts in timing and amount of crop residue burnt. *Environmental Research Letters*, **15**(10), p. 104067. DOI: https://doi.org/10.1088/1748-9326/aba714.

Singh, K., 2009. Act to Save Groundwater in Punjab: Its Impact on Water Table, Electricity Subsidy and Environment. *Agricultural Economics Research Review*, **22**(conf), pp. 365-386. DOI: https://doi.org/10.22004/ag.econ.57482

Singh, V., Singh, S., Biswal, A., Kesarkar, A.P., Mor, S. and Ravindra, K., 2020. Diurnal and temporal changes in air pollution during COVID-19 strict lockdown over different regions of India. *Environmental Pollution*, **266**, p. 115368. DOI: https://doi.org/10.1016/j.envpol.2020.115368.

Singh, V., Singh, S. and Biswal, A., 2021. Exceedances and trends of particulate matter (PM$_{2.5}$) in five Indian megacities. *Science of the Total Environment*, **750**, p. 141461. DOI: https://doi.org/10.1016/j.scitotenv.2020.141461.

Stirling, E.L., Pope, R.J., Graham, A.M., Chipperfield, M.P. and Arnold, S.R., 2020. Quantifying the transboundary contribution of nitrogen oxides to UK air quality. *Atmospheric Science Letters*, **21**(2), p. 955. DOI: https://doi.org/10.1002/asl.955.

Tang, L., Rayner, D., Haeger-Eugensson, M., 2011. Have meteorological conditions reduced NO2 concentrations from local emission sources in gothenburg? *Water. Air, & Soil Pollution*, **221**, pp. 275–286. DOI: https://doi.org/10.1007/s11270-011-0789-6.

Wehner, B., Birmili, W., Ditas, F., Wu, Z., Hu, M., Liu, X., Mao, J., Sugimoto, N. and Wiedensohler, A., 2008. Relationships between submicrometer particulate air pollution and air mass history in Beijing, China, 2004–2006. *Atmospheric Chemistry and Physics*, **8**(20), pp. 6155-6168. DOI: https://doi.org/10.5194/acp-8-6155-2008.

Van Geffen, J.H.G.M., Boersma, K.F., Van Roozendael, M., Hendrick, F., Mahieu, E., De Smedt, I., Sneep, M. and Veefkind, J.P., 2015. Improved spectral fitting of nitrogen dioxide from OMI in the 405–465 nm window. *Atmospheric Measurement Techniques*, **8**(4), pp. 1685-1699. DOI: https://doi.org/10.5194/amt-8-1685-2015.

van Geffen, J. H. G. M., Eskes, H. J., Boersma, K. F., Maasakkers, J. D., and Veefkind, J. P.: TROPOMI ATBD of the total and tropospheric NO$_2$ data products, Report S5P-KNMI-L2-0005-RP, version 1.4.0, released 6 February 2019, KNMI, De Bilt, the Netherlands, available at: http://www.tropomi.eu/documents/atbd/, last access: 10 March 2021.

Wiedinmyer, C., Akagi, S.K., Yokelson, R.J., Emmons, L.K., Al-Saadi, J.A., Orlando, J.J. and Soja, A.J., 2011. The Fire INventory from NCAR (FINN): A high resolution global model to estimate the emissions from open burning. *Geoscientific Model Development*, **4**(3), pp. 625-641. DOI: https://doi.org/10.5194/gmd-4-625-2011.

Zhang, T., De Jong, M.C., Wooster, M.J., Xu, W. and Wang, L., 2020. Trends in eastern China agricultural fire emissions derived from a combination of geostationary (Himawari) and polar (VIIRS)

orbiter fire radiative power products. *Atmospheric Chemistry and Physics*, **20**(17), pp. 10687-10705.
775   DOI: https://doi.org/10.5194/acp-20-10687-2020.

Figures:

780

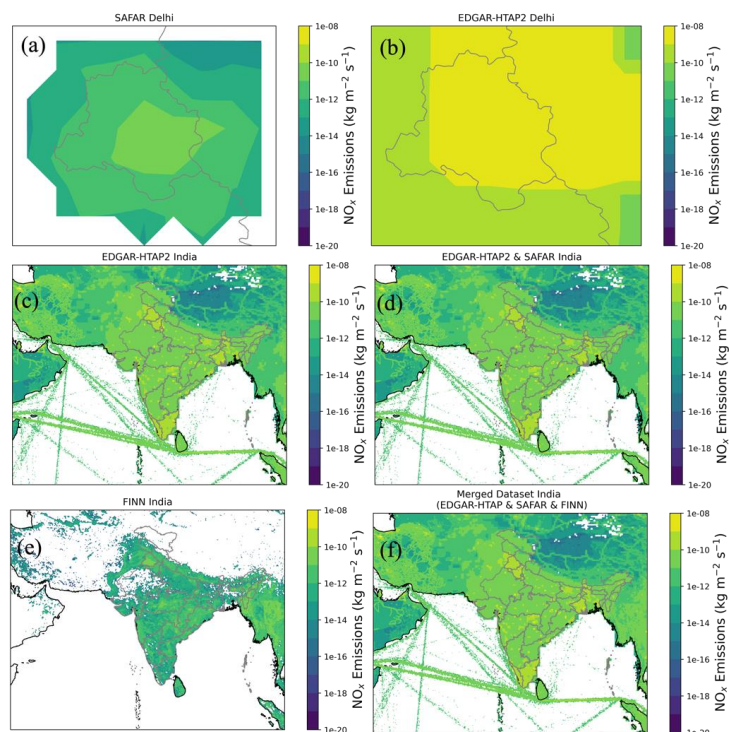**Figure 1. (a) NO$_x$ emissions (kg m^{-2} s^{-1}) within Delhi from the System of Air Quality and Weather Forecasting And Research (SAFAR) (Beig, 2018) for 2018 regridded from 400 m to 10 km resolution. (b) NO$_x$ emissions within Delhi from the Emission Database for Global Atmospheric Research with Task Force on Hemispheric Transport of Air Pollution version 2.2 (EDGAR-HTAP2) (Janssens-Maenhout et al., 2015) emissions for 2010 at 10 km resolution. (c) Global NO$_x$ emissions from EDGAR-HTAP2 for 2010 at 10 km resolution. (d) Merged EDGAR-HTAP2 and SAFAR NO$_x$ emissions, where EDGAR-HTAP2 NO$_x$ emissions within Delhi have been replaced with NO$_x$ emissions from SAFAR. (e) Global fire emissions provided by the FINNv2.5 dataset for 2018 at 10 km resolution. (e) Merged anthropogenic and fire NO$_x$ emissions dataset, where SAFAR, EDGAR-HTAP2 and FINNv2.5 emissions have been combined.**
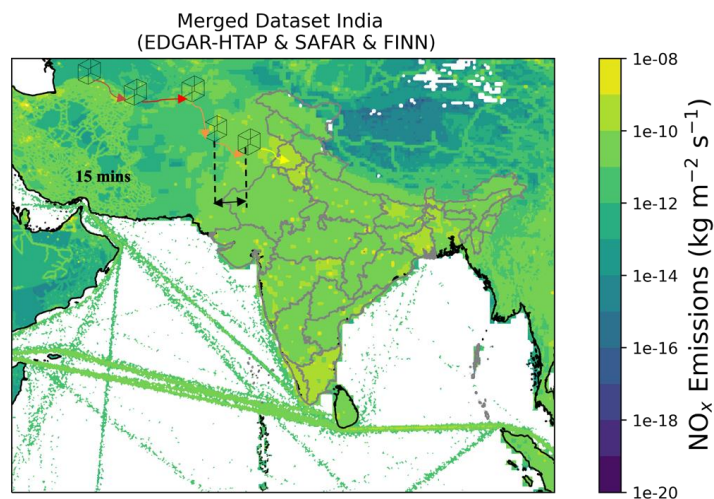
Figure 2. Back-trajectory method used in this study. Gridded emissions from a bottom-up inventory (Figure 1e) are summed every 15-minutes (15 mins) along the back-trajectory path (arrows) when the air parcel is within the boundary layer (indicated by boxes). NO$_x$ accumulates along the trajectory path towards Delhi (indicated by line shading). Satellite tropospheric column NO$_2$ (TCNO$_2$) is also summed in a similar way.
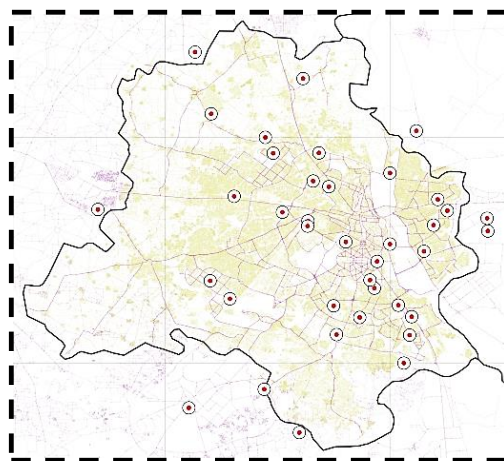
Figure 3. Map showing the location of NO$_2$ monitoring sites over Delhi. In this study we use the daily 07:30-08:30 UTC (13:00-14:00 local time) median NO$_2$ concentration (calculated using all sites shown) to determine the timing of high pollution days in Delhi. We define high pollution days as days where the NO$_2$ concentration exceeds the 90th percentile of NO$_2$ concentrations between 2018 and 2019.
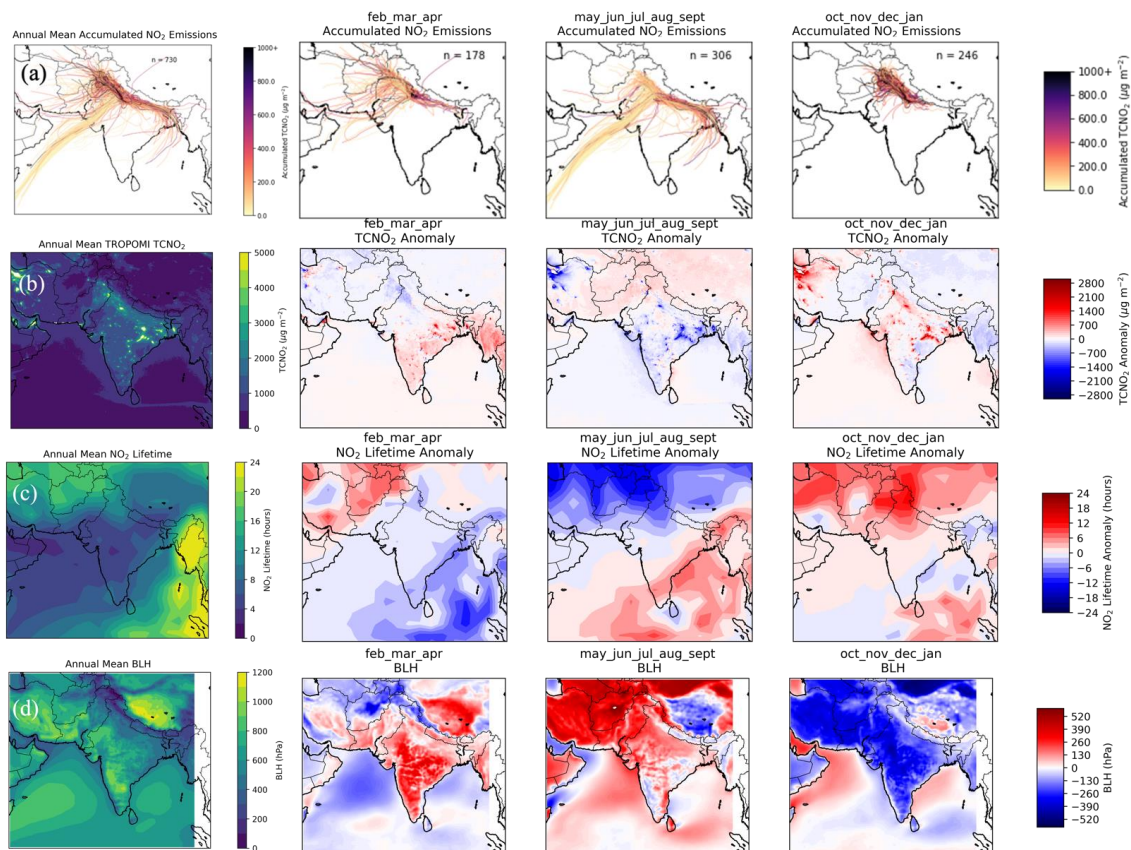
Figure 4. (a) Total annual (and seasonal) accumulated TROPOMI TCNO$_2$ (µg m^{-2}) arriving in Delhi along 4-day back trajectories. Trajectories are coloured by their total accumulated TCNO$_2$, with darker trajectories indicating higher levels of accumulated TCNO$_2$. (b) Mean annual (and seasonal) TCNO$_2$ (anomaly) (µg m^{-2}), (c) mean annual (and seasonal) NO$_2$ lifetime (anomaly) (hours) and (d) mean annual (and seasonal) boundary layer height (BLH) (anomaly) (hPa) compared to all seasons. All panels show the time period of 2017 and 2018 annually and seasonally - during the pre-monsoon (Feb_Mar_Apr), monsoon (May_Jun_Jul_Aug_Sept) and post-monsoon (Oct_Nov_Dec_Jan) seasons, respectively.

795
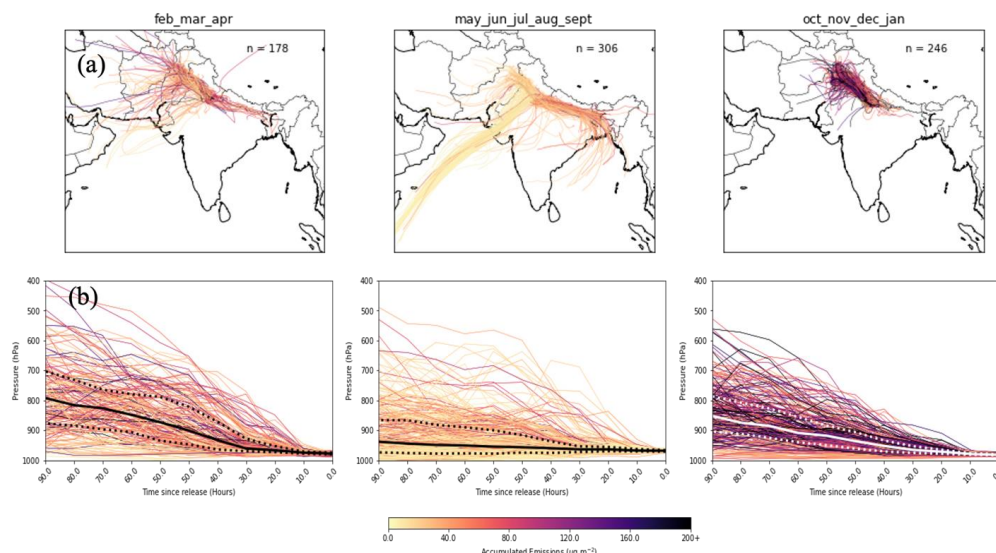
Figure 5. (a) Total accumulated NO$_x$ emissions (µg m^{-2}) arriving in Delhi in 2017 and 2018 and (b) pressure level of air parcels as they converge on Delhi, just above the surface (~1000 hPa) at hour 0 in pre-monsoon (Feb_Mar_Apr), monsoon (May_Jun_Jul_Aug_Sept) and post-monsoon (Oct_Nov_Dec_Jan) seasons. Median (black/white line), 25th and 75th percentiles (black/white dashed lines) of the trajectory pressure are also indicated. Trajectories are coloured by their total accumulated emissions, with darker trajectories indicating higher levels of accumulated NO$_x$.
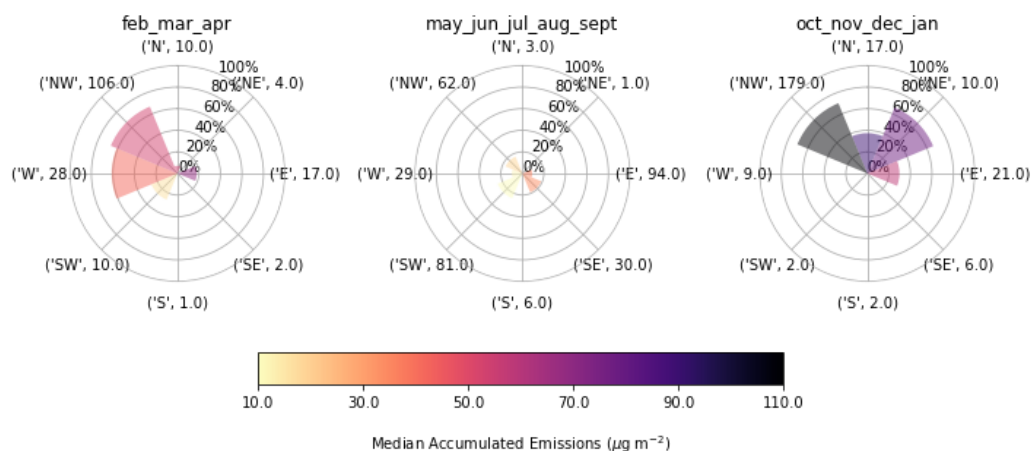
Figure 6. Wind rose of median accumulated NO$_x$ emissions (µg m^{-2}) from 4-day back trajectories with 6-hr time steps arriving at Delhi in 2017 and 2018 for pre-monsoon (Feb_Mar_Apr), monsoon (May_Jun_Jul_Aug_Sept) and post-monsoon (Oct_Nov_Dec_Jan) seasons. Total accumulated emissions are indicated by the shading of the segments. The area of the segment indicates the non-local contribution to the total integrated emissions. The percentage of local emissions is indicated on the circles. The number of days on which each wind direction occurs in each season is also indicated in brackets. For example, NW in the post-monsoon is very polluted (~100 µg m^{-2}), 70% of total integrated emissions are non-local and this wind direction occurs on 179 days.
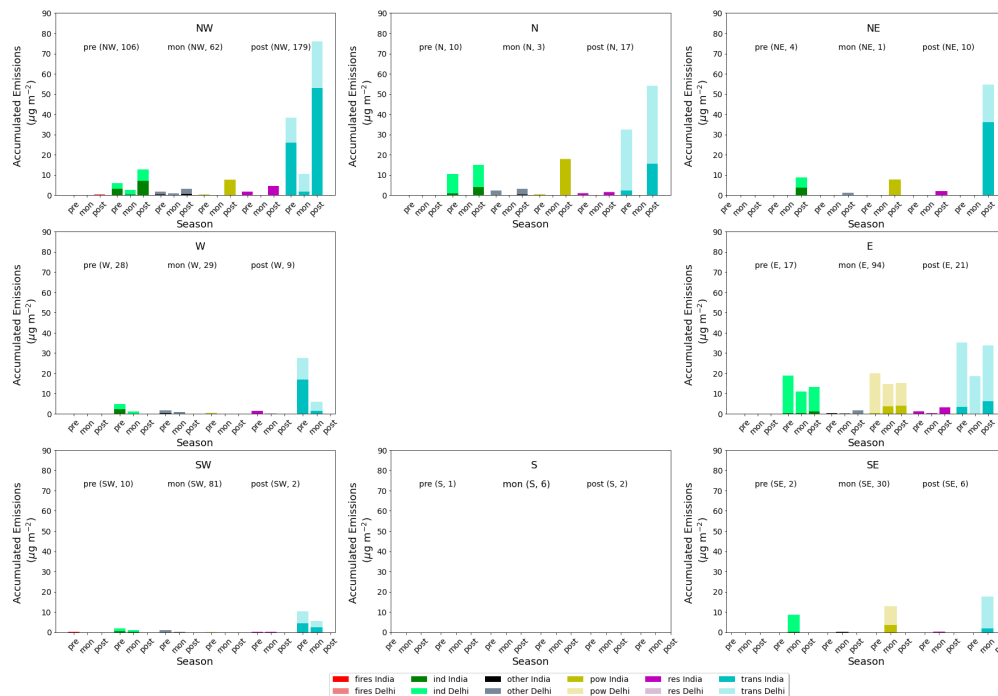
Figure 7. Sector-specific accumulated NO$_x$ emissions (μg m^{-2}) from 4-day back trajectories with 6-hr time steps arriving in Delhi in 2017 and 2018 in pre-monsoon (pre) (Feb_Mar_Apr), monsoon (mon) (May_Jun_Jul_Aug_Sept) and post-monsoon (post) (Oct_Nov_Dec_Jan). Light shading indicates accumulated NO$_x$ emissions originating within Delhi and darker shading indicates accumulated NO$_x$ emissions originating from outside of Delhi. Sectors included are fire (FIRES) (red), industrial (IND) (green), other (OTHER) (black), power generation (POW) (gold), residential (RES) (magenta) and transportation (TRANS) (cyan) emissions. The number of days for which each wind direction occurs in each season is indicated in brackets. For example, north-westerly winds occur on 179 days during the post-monsoon and transport emissions dominate (~80 μg m^{-2}). The contribution from transport is split into ~55 μg m^{-2} that are non-local (India) and ~25 μg m^{-2} that are local (Delhi).

800

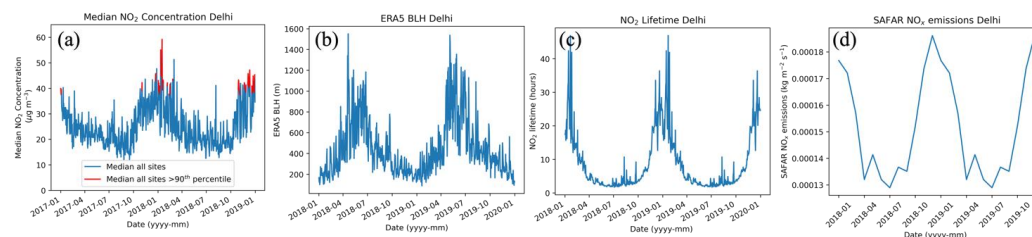**Figure 8. (a) Daily median NO$_2$ concentrations (μg m^{-3}) in Delhi (blue). Concentrations above the 90th percentile of observations are indicated in red. (b) Daily mean boundary layer height (BLH) (m) in Delhi from ERA5 re-analysis, (c) Daily mean NO$_x$ lifetime (hours) in Delhi and (d) Monthly mean NO$_x$ emissions (kg m^{-2} s^{-1}) from the SAFAR emissions inventory. All panels show the time-period between 1st January 2017 and 31st December 2018.**
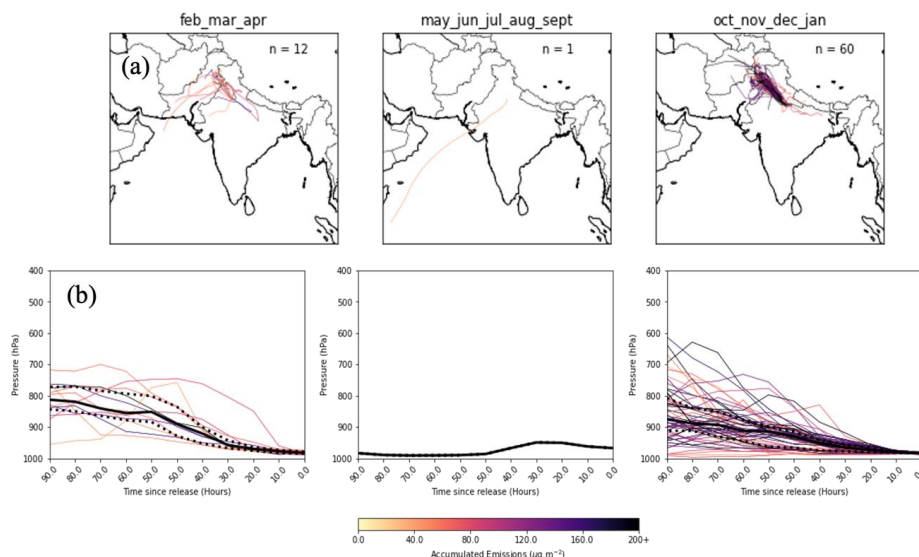
Figure 9. (a) Total accumulated NO$_x$ emissions (µg m^{-2}) arriving at Delhi during high pollution events in in 2017 and 2018, **(b)** pressure level of air parcels as they converge on Delhi just above the surface (~1000 hPa) at hour 0 in pre-monsoon (Feb_Mar_Apr), monsoon (May_Jun_Jul_Aug_Sept) and post-monsoon (Oct_Nov_Dec_Jan). Median (black line), 25th and 75th percentiles (black dashed lines) of the trajectory pressure are also indicated. Trajectories are coloured by their total accumulated emissions, with darker trajectories indicating higher levels of accumulated NO$_x$.
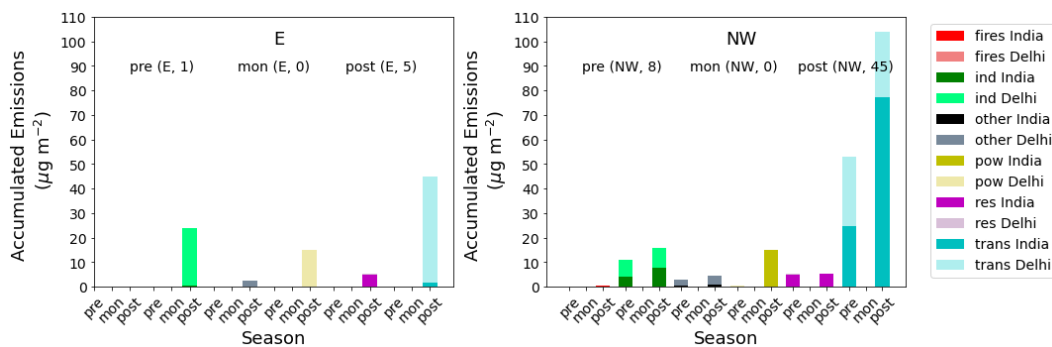

Figure 10. Sector-specific accumulated NO$_x$ emissions (µg m^{-2}) from 4-day back trajectories with 6-hr time steps arriving at Delhi during high pollution events in 2017 and 2018 in the pre-monsoon (pre) (Feb_Mar_Apr), monsoon (mon) (May_Jun_Jul_Aug_Sept) and post-monsoon (post) (Oct_Nov_Dec_Jan). Light shading indicates accumulated NO$_x$ emissions originating within Delhi and darker shading accumulated NO$_x$ emissions from outside of Delhi. Sectors included are fire (FIRES) (red), industrial (IND) (green), other (OTHER) (black), power generation (POW) (gold), residential (RES) (magenta) and transportation (TRANS) (cyan) emissions. The number of days for which each wind direction occurs in each season is indicated in brackets. For example, north-westerly winds occur on 45 days during high pollution days in the post-monsoon and transport emissions dominate (>100 µg m^{-2}). The contribution from transport is split into ~80 µg m^{-2} that are non-local (trans India) and ~25 µg m^{-2} that are local (trans Delhi).

805

Season	Dominant wind direction (% of days)	Key Source Sectors (% contribution)	Local/non-local contribution to accumulated emissions for Key Source Sector (% contribution)
Pre-monsoon	NW (54%)	Transport (80%)	Local (32%)/Non-local (68%)
Monsoon	E (31%)	Transport (42%) Power (32%) Industry (25%)	Local (91%)/Non-local (9%) Local (98%)/Non-local (2%) Local (98%)/Non-local (2%)
	SW (27%)	Transport (81%)	Local (59%)/Non-local (41%)
	NW (20%)	Transport (73%)	Local (84%)/Non-local (16%)
Post-monsoon	NW (73%)	Transport (73%)	Local (30%)/Non-Local (70%)

Table 1s. Summary of key wind-directions in the pre-monsoon (Feb-Apr), monsoon (May-Sept) and post-monsoon (Oct-Jan) monsoon (as % of total days in each season). The key source sectors with the largest contribution to the overall total accumulated emissions are also indicated (as % contribution) alongside the contribution of local (Delhi) and non-local (rest of India) accumulated emissions to overall accumulated emissions for that sector. For example, in the post-monsoon NW winds occur 73% of days, transport emissions contribute 72% of the overall integrated emissions and 30% of transport emissions are local, while 70% are non-local. Seasonal sector-specific accumulated NO$_x$ emissions (μg m^{-2}) are calculated from 4-day back trajectories with 6-hr time steps arriving in Delhi in 2017 and 2018 in pre-monsoon, monsoon and post-monsoon periods.

810

815